Journal of Power Sources 192 (2009) 151–157

Contents lists available at ScienceDirect

Journal of Power Sources

journal homepage: www.elsevier.com/locate/jpowsour

Chemical compatibility between YSZ and SDC sintered at different atmospheres for SOFC applications

Ana Martínez-Amesti [a], Aitor Larrañaga [a,*], Lide M. Rodríguez-Martínez [b], Mª Luisa Nó [a], Jose L. Pizarro [a], Ander Laresgoiti [b], Mª Isabel Arriortua [a]

[a] Facultad de Ciencia y Tecnología, UPV/EHU, Apdo. 644, E-48080 Bilbao, Spain
[b] Ikerlan, Centro Tecnológico, Juan de la Cierva 1, Miñano 01510, Álava, Spain

ARTICLE INFO

Article history:
Received 15 October 2008
Received in revised form 4 February 2009
Accepted 5 February 2009
Available online 13 February 2009

Keywords:
SOFC
Zirconia
Ceria
Diffusion

ABSTRACT

Doped ceria barrier layers have extensively been used between Fe and/or Co containing cathode materials and conventional yttria-stabilized zirconia (YSZ) electrolytes in Solid Oxide Fuel Cells (SOFCs) to improve performance and prevent unwanted chemical reactions between them. However, the chemical compatibility between the YSZ and doped ceria depends strongly on the sintering temperature and atmosphere. This study focuses on the influence of temperature and sintering atmosphere in the crystal structure, microstructure and conductivity of bulk mixtures of YSZ and $Sm_{0.2}Ce_{0.8}O_{1.9}$ (SDC). Polycrystalline mixtures of YSZ–SDC (50% weight) were sintered between 950 and 1350 °C in air, Ar and hydrogen containing reducing atmospheres. X-ray powder diffraction (XRD), scanning electron microscopy (SEM), energy dispersive X-ray analysis (EDX) and electrochemical impedance spectroscopy (EIS) were used to analyse the chemical interactions between SDC and YSZ under different processing conditions. Overall, diffusion between SDC and YSZ is observed for all cases but the solid solution formed depends upon the temperature and the sintering atmosphere. The additional formation of $(Ce,Sm)_2Zr_2O_7$ pyrochlore is observed when sintering under reducing atmosphere. SEM and EDX analysis reveal microstructure variations with higher homogeneity for the samples sintered in argon or hydrogen. The sintering behaviour and the total conductivity properties are also dependent on sintering atmospheres, showing that inert conditions may yield the best performing YSZ–SDC system for SOFC applications.

1. Introduction

In the last few years, ceria-based electrolytes are presented as interesting substitutes of traditional YSZ electrolytes in Solid Oxide Fuel Cells (SOFCs) operating at temperatures below 600 °C. The partial substitution of Ce^{4+} ion by trivalent cations such as Gd^{3+}, Sm^{3+}, Y^{3+} or La^{3+} enhances the chemical stability, increases the ionic conductivity and decreases the reduction of ceria materials [1–5], the last factor may depend on the type and content of the trivalent dopant cation. In this context, many systems have been studied, such as CeO_2–Sm_2O_3, CeO_2–Gd_2O_3 and CeO_2–Y_2O_3 [6].

Currently, the ceria-based materials are used as electrolyte, but also as a reaction barrier layer between the yttria-stabilized zirconia (YSZ) electrolyte and cathode materials (LSF, LSCF) or, as a barrier between the anode (NiO–YSZ) and YSZ electrolyte of SOFC components.

The objective of the ceria barrier layer between the cathode and electrolyte is to prevent the formation of poorly conducting secondary phases, such as $La_2Zr_2O_7$ or $SrZrO_3$ [7,8], with less favourable properties for their cathode function in SOFC cells [9].

The aim of this work is to study the influence of processing atmosphere and temperature in the chemical interaction between the SDC and YSZ materials and its effects in relevant properties for their applications in SOFC's electrodes. Detailed X-ray powder diffraction (XRD) study, scanning electron microscopy (SEM), energy dispersive X-ray analysis (EDX) and electrochemical impedance spectroscopy (EIS) were carried out on polycrystalline mixtures sintered under different atmospheres and temperatures.

2. Experimental

The materials used in this study were yttria-stabilized zirconia $(ZrO_2)_{0.92}$ $(Y_2O_3)_{0.08}$ (YSZ), SSA = 13 $m^2\ g^{-1}$ d_{50} = 0.54 μm powders from Tosoh Corporation and samarium doped ceria, $Ce_{0.8}Sm_{0.2}O_{1.9}$ (SDC), SSA = 14 $m^2\ g^{-1}$ d_{50} = 0.60 μm from Praxair Surface Technologies.

* Corresponding author. Tel.: +34 946012599; fax: +34 946013500.
E-mail address: aitor.larranaga@ehu.es (A. Larrañaga).

0378-7753/$ – see front matter © 2009 Elsevier B.V. All rights reserved.
doi:10.1016/j.jpowsour.2009.02.011

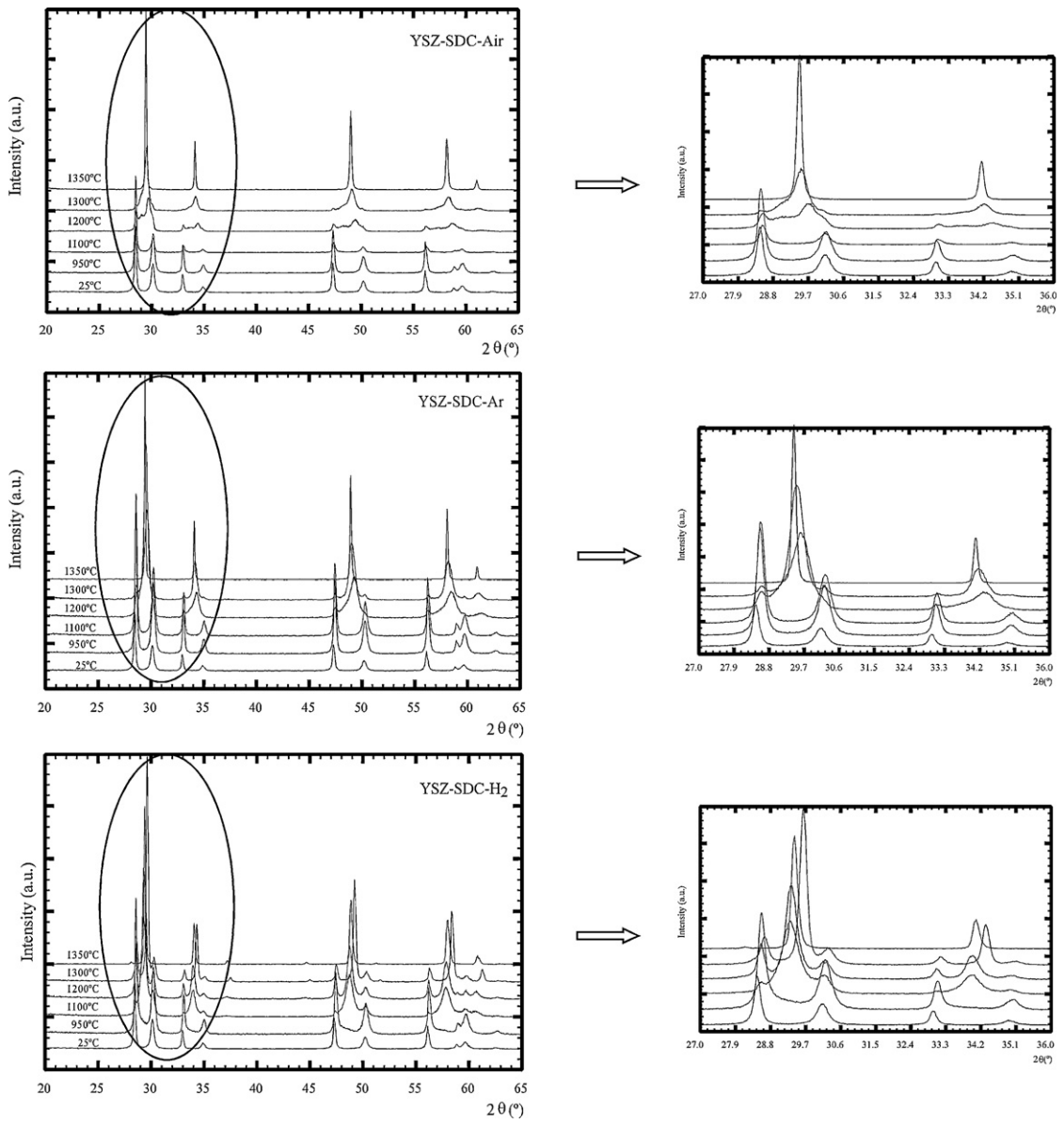

Fig. 1. Room temperature X-ray powder diffraction patterns of YSZ and SDC mixtures prepared at different temperatures (25, 1100, 1200, 1300 and 1350 °C) and atmospheres (air, argon and hydrogen).

The diffusion study between YSZ and SDC materials at different atmospheres and temperatures has been carried out using the following procedure: to assure homogeneity of the SDC and YSZ 50/50% weight polycrystalline mixtures, attrition milling was employed using an Attritor 01-HD mill. Starting from 10 g of each sample with 220 g of zirconia 2 mm ball media and 25 ml of acetone in a 100 cc vessel, the mixtures were milled at 500 rpm during 30 min and then the solvent was evaporated. The obtained powders were used to prepare pellets pressed at 6 tons for 1 min using 13 mm diameter die and 1 g of powder mixture in a uniaxial press Specac.

Pellets were sintered in a conventional Carbolite tubular furnace at different atmospheres (containing air, argon and hydrogen) and temperatures (950, 1100, 1200 and 1300 for 2 h and 1350 °C for 5 h) using 3 °C min^{-1}-heating speed. Powders thus obtained were studied by X-ray powder diffraction recorded at room temperature, using a PHILIPS X'PERT automatic diffractometer, equipped with Cu-Kα radiation (λ = 1.5418 Å). The power generator has been provided at 40 kV and 40 mA. The patterns were recorded in 2θ steps of 0.02° in the 10–70° range, counting for 1 s per step.

Electrochemical impedance spectroscopy measurements were used to study the influence of sintering atmosphere in the conductivity of SDC–YSZ mixtures. Cylindrical pellets (13 mm diameter) of initial powder mixtures were uniaxially pressed at 6 tons and then isostatically pressed at 20 tons. These pellets were then sintered in air, argon and hydrogen containing atmospheres at 1350 °C for 5 h using a heating/cooling rate of 3 °C min^{-1}. Sintered pellets were cut and polished into small rectangular bars of approximate 13 mm × 1 mm × 1 mm dimensions. Pt paste and Pt leads were place over the polished surfaces for electrical contact points and fired at 950 °C for 30 min.

Electrochemical measurements were performed with a Solartron 1260 frequency response analyzer coupled to a Solartron 1286 electrochemical interface, with AC voltage amplitudes of 250 mV over a frequency range of 0.01–10^6 Hz and between 400 and 900 °C every 100 °C.

The microstructure and composition analysis of bulk polycrystalline bars was carried out using a JEOL-6400 Scanning Electron Microscope instrument equipped with and Oxford Inca Pentafet X3 energy dispersive X-ray analyzer. Samples for SEM and EDX were

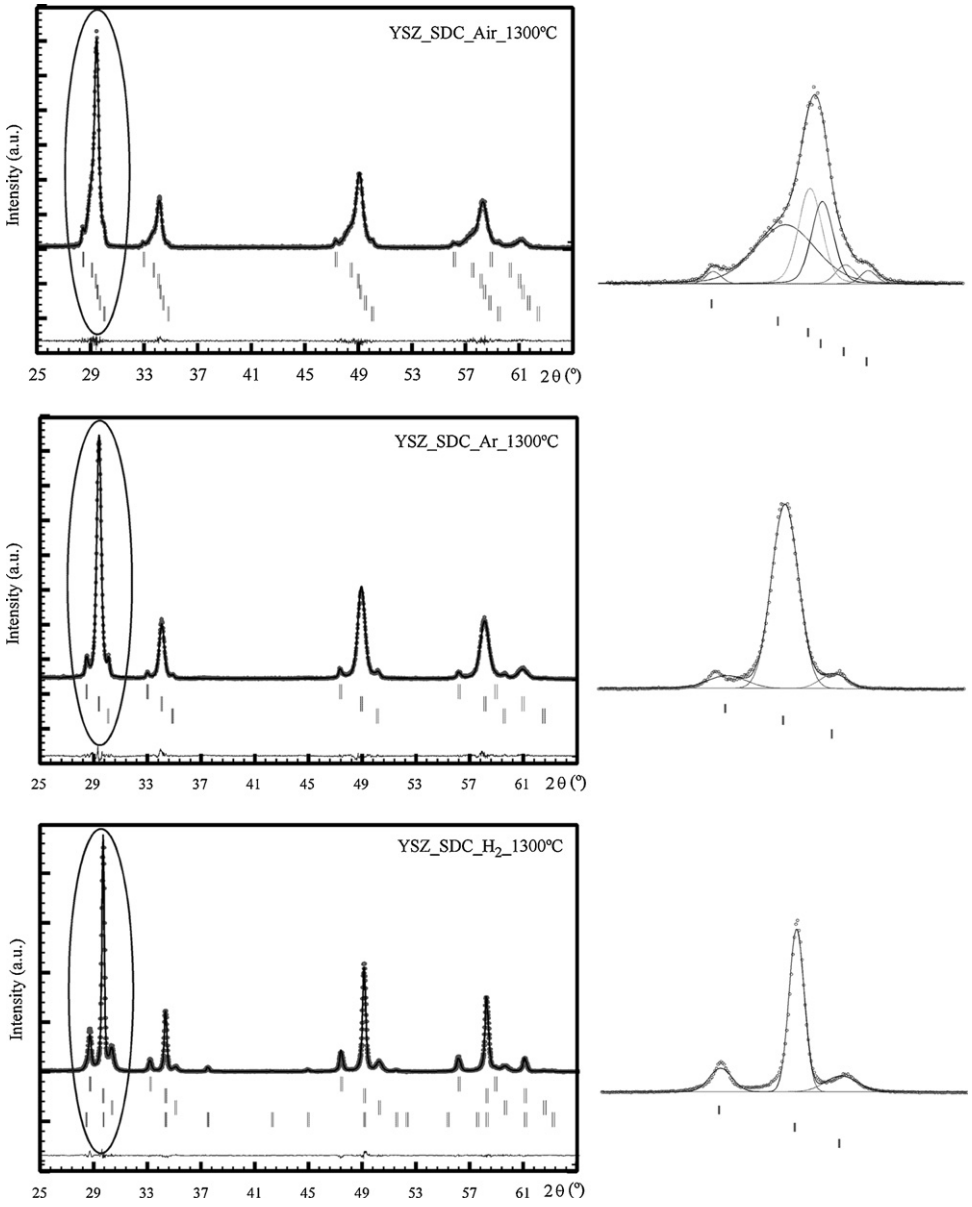

Fig. 2. Full-profile refinement and the deconvolution of the initial peaks for the samples treated at 1300 °C in air, argon and hydrogen.

embedded in epoxy resin prior to cut and polished using standard metallographic techniques and they were coated with a coal Graphite layer deposited by evaporation (BAL-TEC SCD 004 Sputter Coater).

3. Results and discussion

3.1. Room temperature X-ray powder diffraction analysis

Polycrystalline YSZ–SDC samples prepared at different temperatures and atmospheres were studied by X-ray powder diffraction (Fig. 1) and refined using the full-profile refinement with structural model (Rietveld method) by FullProf [10–12]. Preliminary identification of the initial oxides and the formation of new phases were evaluated using the Powder Diffraction File (PDF) database. In all the cases, the deconvolution of the initial two diffraction maxima (at ~28° and 31° in 2θ) provides an indication of the number of phases present in each XRD diagram. This procedure was carried out using the peak-fit option of the WinPLOTR program without structural model. The simulated profiles were then used to recalculate the starting unit cell parameters from the 2θ peak positions.

Once the present phases were identified and the starting unit cell parameters were obtained, the Rietveld method allowed the quantitative analysis of each individual phase observed for each XRD pattern at different processing temperatures and atmospheres (Fig. 2). Generally it is not possible to determine the exact crystal structure in a solid solution. But in this particular case with YSZ–SDC mixtures is possible to quantify the exact weight proportion and exact composition of each phase. The starting compounds have the same crystal structure and all its atoms are in special positions on symmetry elements. This particular situation allows the full-profile refinement with structural model, using two cycling variables that affect the intensity of the X-ray powder diagrams. (1) The scale factor that let us to quantify the weight proportion of each phase. (2) The occupation factor of the replaced atom (Ce–Zr) that let us to quantify the ceria zirconia relationship for each phase.

So, in this case the quantitative analysis of the mixtures without using any restriction in the X-ray refinement allows obtaining weight and composition values for each phase.

Table 1
Results from XRD Rietveld analysis for SDC–YSZ powder mixtures as a function of sintering atmosphere and temperature. Data of identified phases are included for each atmosphere and temperature combination. Phase quantification in weight % is included in brackets.

Atmosphere	Temperature (°C)					
	25	950	1100	1200	1300	1350
Air	SDC [48] YSZ [52]	SDC [48] YSZ [52]	SDC [37] $(SDC)_{0.95}(YSZ)_{0.05}$ [8] $(SDC)_{0.29}(YSZ)_{0.71}$ [8] YSZ [47]	SDC [13] $(SDC)_{0.95}(YSZ)_{0.05}$ [22] $(SDC)_{0.58}(YSZ)_{0.42}$ [5] $(SDC)_{0.35}(YSZ)_{0.65}$ [48] YSZ [12]	SDC [4] $(SDC)_{0.71}(YSZ)_{0.29}$ [29] $(SDC)_{0.59}(YSZ)_{0.41}$ [25] $(SDC)_{0.45}(YSZ)_{0.55}$ [26] $(SDC)_{0.34}(YSZ)_{0.66}$ [12] YSZ [4]	$(SDC)_{0.50}(YSZ)_{0.50}$
Argon	SDC [48] YSZ [52]	SDC [48] YSZ [52]	SDC [48] YSZ [52]	SDC [6] $(SDC)_{0.60}(YSZ)_{0.40}$ [49] $(SDC)_{0.36}(YSZ)_{0.64}$ [41] YSZ [4]	SDC [4] $(SDC)_{0.51}(YSZ)_{0.49}$ [91] YSZ [5]	$(SDC)_{0.51}(YSZ)_{0.49}$
Hydrogen	SDC [48] YSZ [52]	SDC [40] $(SDC)_{0.95}(YSZ)_{0.05}$ [16] YSZ [44]	SDC [4] $(SDC)_{0.61}(YSZ)_{0.39}$ [63] YSZ [16] $(Ce,Sm)_2Zr_2O_7$ [17]	SDC [13] $(SDC)_{0.56}(YSZ)_{0.44}$ [49] YSZ [16] $(Ce,Sm)_2Zr_2O_7$ [22]	SDC [13] $(SDC)_{0.49}(YSZ)_{0.51}$ [46] YSZ [15] $(Ce,Sm)_2Zr_2O_7$ [26]	$(SDC)_{0.49}(YSZ)_{0.51}$ [53] $(Ce,Sm)_2Zr_2O_7$ [47]

Fig. 2 shows a good agreement between the structural model and experimental data, indicating a successful characterization and quantification of the phases present at 1300 °C under different processing atmospheres.

As an overall result of these detailed XRD analyses, there exist a chemical interaction between YSZ and SDC that varies as a function of sintering temperature and atmosphere. The compositional gradient formed between the starting layers due to the diffusion of CeO_2 and ZrO_2 depends strongly upon the processing atmosphere as shown in Table 1. This effect started at 950 °C when the sintering was made under hydrogen containing atmosphere, at 1100 °C when air was used and at 1200 °C when argon was used indicating that reactivity can be delayed to higher temperature by modifying the processing atmosphere.

For samples sintered under hydrogen containing atmosphere over 1100 °C, there is the formation of a secondary $(Ce,Sm)_2Zr_2O_7$ pyrochlore phase [13], as a consequence of the Ce^{4+} to Ce^{3+} reduction. The x fraction of the solid solution $(SDC)_x(YSZ)_{1-x}$ formed under hydrogen reducing processing conditions decreases as temperature increases, probably due to the enhanced formation of the $(Ce,Sm)_2Zr_2O_7$ phase at higher temperatures. However, only one $(SDC)_x(YSZ)_{1-x}$ phase per processing temperature is identified under hydrogen sintering.

When samples are sintered under inert or oxidizing atmospheres a compositional $(SDC)_x(YSZ)_{1-x}$ gradient is formed, with a wider x distribution for samples processed in air. At 1300 °C, only one $(SDC)_{0.5}(YSZ)_{0.5}$ phase is present in mixtures processed in argon. At this temperature, the distribution of $(SDC)_x(YSZ)_{1-x}$ phases formed in air becomes narrower than at lower temperature. The reaction between SDC and YSZ moves towards the formation of only one intermediate $(SDC)_{0.5}(YSZ)_{0.5}$ single phase when exposed to even higher temperatures (1350 °C) and longer sintering times (5 h).

The evolution of unit cell parameters of these two fluorite type structural phases (SDC and YSZ) as a function of temperature are represented in Fig. 3, for different processing atmospheres.

The variation of unit cell parameters with temperature starts to be significant over 950 °C for both YSZ and SDC. In the case of the decrease in cell parameters can be related with the diffusion of Zr^{4+} cations in the crystal network of SDC [14] in good agreement with the smaller size of Zr^{4+} (0.84 Å) in contrast with Ce^{4+} (0.97 Å) [15]. As well, an increase in the cell parameters of YSZ at high temperature is consistent with the diffusion of Ce^{4+} cations into the YSZ crystal lattice. This Ce–Zr interdiffusion may indicate the facility towards solid solution formation under different atmospheres. The extent of lattice parameters variation is most marked for those samples fired under oxidant atmosphere (air). However, this variation over temperature is less significant for mixtures sintered in reducing atmospheres, which may indicate that the reduction of cerium decreases the cross-migration between phases and favours the formation of the pyrochlore structure.

Fig. 4 shows the cell parameters for each $(SDC)_x(YSZ)_{1-x}$ solid solution with cubic structure as a function of x and the sintering atmosphere.

The unit cell parameters of the solid solution compounds follow the same behaviour as the composition $(SDC)_x(YSZ)_{1-x}$ at different sintering atmospheres, indicating that the resulting products from the diffusion of Ce^{4+} and Zr^{4+} cations are heavily dependent on temperature and less of the atmosphere.

3.2. Scanning electron microscopy and energy dispersive X-ray analysis

The SEM micrographs obtained by Secondary Electron Detector using 20 kV (Fig. 5) show the surface microstructure sintered at 1350 °C during 5 h and under different atmospheres. Initial powder mixtures, pressing and processing conditions and temperature were identical and therefore, any variations can be attributed to the influence of the atmosphere used in the sintering process.

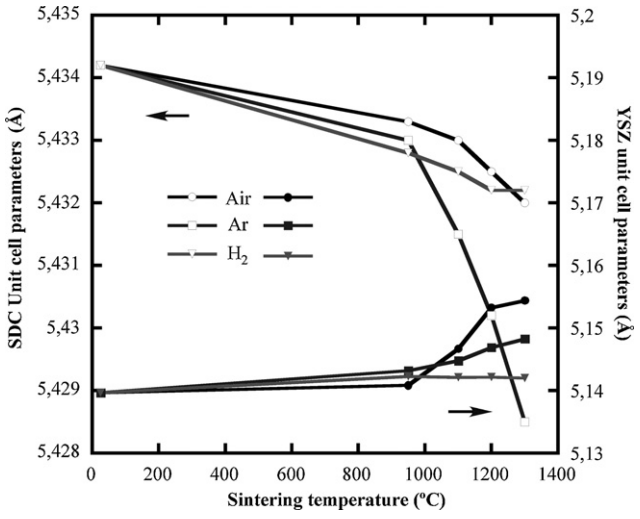

Fig. 3. Unit cell parameters change of YSZ and SDC using different sintering atmospheres.

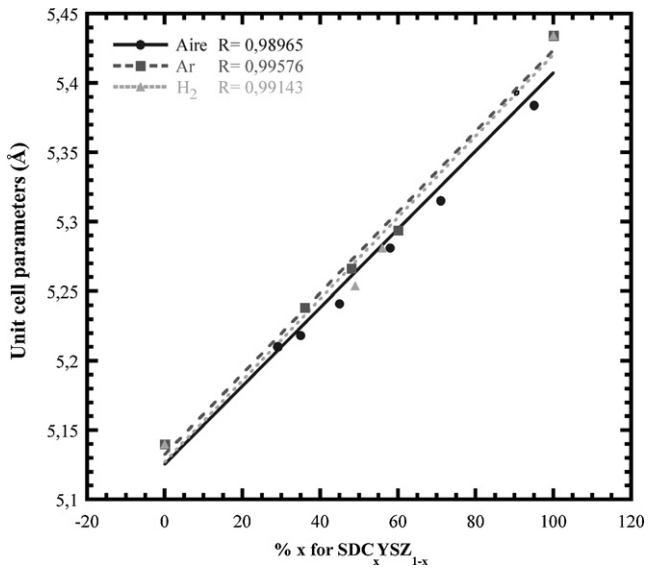

Fig. 4. Cell parameters of each compositional gradient solid solution compound according to the proportion $(SDC)_x(YSZ)_{1-x}$. Data obtained from all the used temperatures.

The degree of sinterability and grain growth is clearly influenced by the processing atmosphere. Fig. 5a corresponds to the surface image for the mixture sintered in air, showing poor sinterability between these particles remaining dispersed and leaving many gaps between grains. Fig. 5b shows the surface microstructure for the sample sintered in argon with high sinterability and connection between grains. Finally, Fig. 5c represents the sample sintered in hydrogen; which qualitatively shows good sinterability but significant pore formation of approximately 0.5 μm in size. These pores can be the result of the volume expansion of the cell as a consequence of the reduction of the cerium from Ce^{4+} (0.97 Å) to Ce^{3+} (1.034 Å) and the formation of the $(Ce,Sm)_2Zr_2O_7$ phase.

Elemental distribution mapping using Energy Dispersive X-ray analysis at 26 kV were performed to check chemical distribution of the phases formed through the sample surface during sintering under different atmospheres (Fig. 6).

The results from this chemical analysis are in good agreement with those obtained by XRD as the most homogeneous chemical distribution corresponds in both cases to the sample sintered in argon (Fig. 6b), followed by the one sintered under hydrogen (Fig. 6c). The sample sintered in air presents a heterogeneous distribution as a consequence of the low sinterability between the particles.

3.3. Electrochemical impedance spectroscopy measurements

AC impedance was used for total conductivity measurements on sintered bars between 400 and 900 °C. These conductivity values have been corrected [16] using the following porosity correction (1)

$$\sigma_{\text{corrected}} = \sigma_{\text{measured}} \left(1 + \frac{pf_{\text{vol}}}{1 - (pf_{\text{vol}})^{2/3}} \right) \quad (1)$$

where pf_{vol} is the pore volume fraction $[pf_{\text{vol}} = 1 - \rho_{\text{exp}}/\rho_{\text{theor}}]$ and $[\rho_{\text{exp}}/\rho_{\text{theor}}]$ are the experimental and theoretical densities obtained from Archimedes Method and X-ray powder diffraction analysis, respectively. The experimental densities were found to be larger that 97% of the theoretical except for the sample sintered in hydrogen, which was 89%.

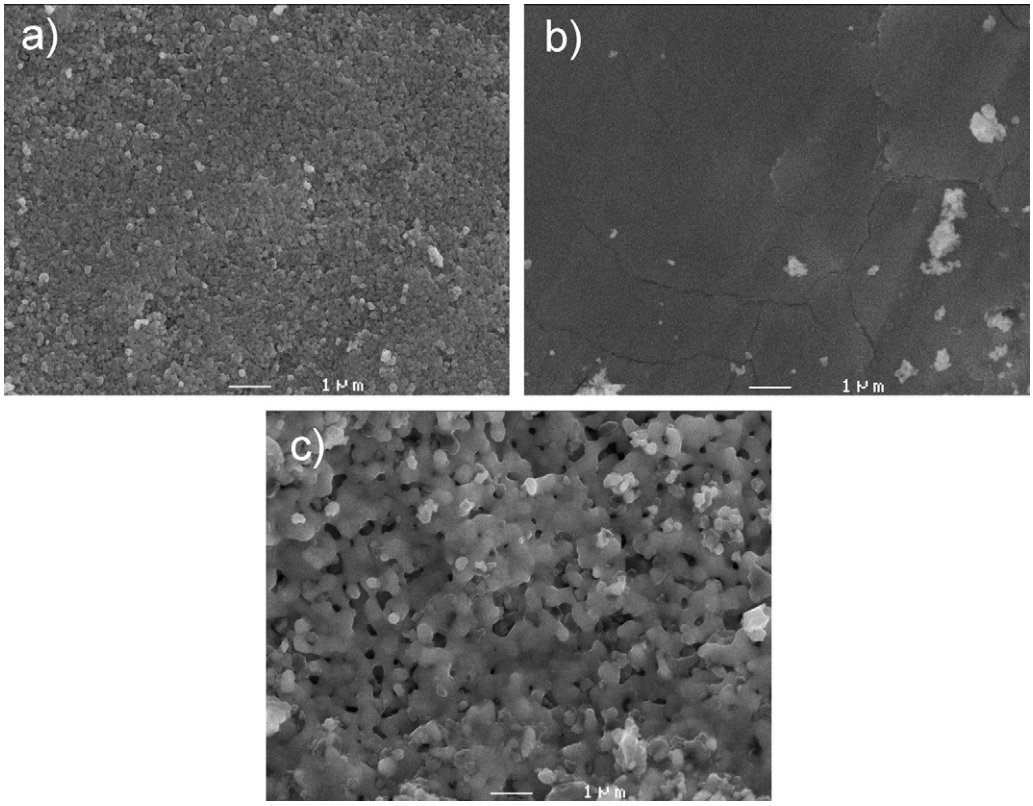

Fig. 5. SEM micrographs for SDC–YSZ samples treated at different atmospheres (a) air, (b) argon and (c) hydrogen.

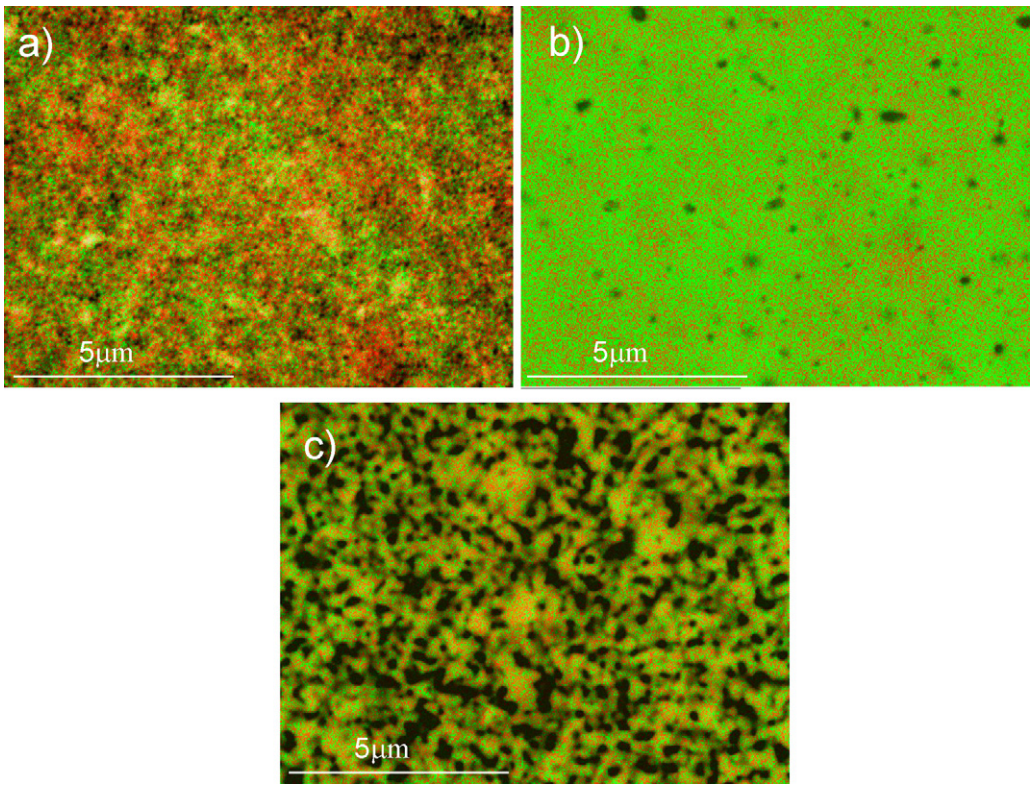

Fig. 6. Element distribution maps by Energy Dispersive X-ray analysis (EDX) for the samples treated at 1350 °C in (a) air, (b) argon and (c) hydrogen. The red regions represent zones with only YSZ, the green colour is associated to SDC and the yellow areas correspond to zones where the Ce and Zr are present simultaneously. (For interpretation of the references to colour in this figure legend, the reader is referred to the web version of the article.)

Fig. 7 shows the conductivity dependence as a function of the inverse of temperature following Eq. (2)

$$\sigma = \frac{\sigma_0}{T}\exp\left(-\frac{E_a}{kT}\right) \quad (2)$$

where σ represents the conductivity, temperature T is in (K^{-1}), k is Boltzman's constant, E_a is the activation energy and σ_0 a pre-exponential factor related to the concentration of charge carriers.

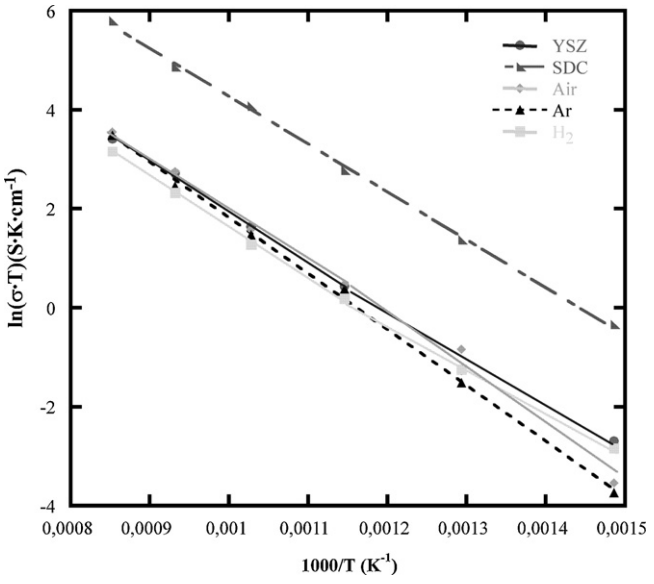

Fig. 7. Electrical conductivity *vs* inverse of temperature measurements for the samples.

The total conductivity consists of a series contribution from the bulk of the grains and from the grain boundaries, which are often very badly conducting. The grain boundary resistance may occur due to segregation of the dopant ions [3]. A detailed characterization of grain boundary and bulk contributions to the total conductivity as a function of temperature and atmosphere is underway. For the time being and looking at its application in SOFCs, total values of conductivity are analysed to determine the relevance of the chemical interaction between YSZ and SDC in conductivity values of mixtures processed under different processing atmospheres.

The sample mixtures show total conductivity values close to those observed for pure YSZ over the studied temperature range and far from pure SDC behaviour. This may indicate that, depending on the extension of this interaction in a multilayer configuration system, the solid solution and impurity formed as a function of the sintering atmosphere may not be the concluding parameters that affect its performance, when the system is based on YSZ. If the reaction penetration is considerable in a system based on SDC, then the conductivity may be significantly affected by these interactions. The layer configuration characterization is also currently under investigation and the results will be published elsewhere.

There is a slight slope change in all curves except for that sintered in argon atmosphere and for pure SDC. Table 2 shows the activation

Table 2
Curvature temperature T_b, activation energy values for conductivities.

Sample	T_b (°C)	E_a ($T<T_b$)	E_a	E_a ($T>T_b$)
YSZ	600	0.79	0.84	0.89
SDC			0.83	
Air	600	1.03	0.97	0.92
Argon			0.97	
Hydrogen	600	0.76	0.82	0.88

energies for each sample along with the curvature temperature (T_b). This is the temperature at which the slope change occurs. The exact cause of this curvature is not known but is generally attributed to the association of defects [17].

Pure YSZ and SDC and the sample sintered in hydrogen show similar activation energies. However the samples sintered in Ar and air show higher values for E_a, which may be associated to certain hindrance of carrier mobility.

4. Conclusions

Diffusion between CeO_2 and YSZ is observed for all cases but the solid solution formed depends upon the temperature and the sintering atmosphere. The additional formation of $(Ce,Sm)_2Zr_2O_7$ pyrochlore is observed when sintering under reducing atmosphere. SEM and EDX analysis reveal microstructure variations with higher homogeneity for the samples sintered in Ar or hydrogen. The sintering behaviour and the total conductivity properties are also dependent on sintering atmospheres, showing that inert conditions may yield the best performing YSZ–SDC system for SOFC applications.

Acknowledgements

This work has been financially supported by the "Departamento de Industria del Gobierno Vasco/Eusko Jaurlaritza", within the strategic actions in Microenergy (GARAZI project, ETORTEK 2007–2009, SAIOTEK 2007 programmes). The authors thank the technicians of SGIker, financed by the "National Program for the Promotion of Human Resources within the National Plan of Scientific Research, Development and Innovation—"Ministerio de Ciencia y Tecnología", "Fondo Social Europeo (FSE)" and "Gobierno Vasco/Eusko Jaurlaritza, Dirección de Política Científica" for the XRD, SEM and EDX measurements. A. Martínez-Amesti wishes to thank the "Gobierno Vasco/Eusko Jaurlaritza, Dirección de Política Científica" and UPV/EHU for funding.

References

[1] B.C.H. Steele, Solid State Ionics 129 (2000) 95.
[2] O. Yamamoto, Electrochim. Acta 45 (2000) 2423.
[3] M. Mogensen, N.M. Sammes, G.A. Tompsett, Solid State Ionics 129 (2000) 63.
[4] D. Pérez-Coll, D. Marrero-López, J.C. Ruiz-Morales, P. Núñez, J.C.C. Abrantes, J.R. Frade, J. Power Sources 173 (2007) 291.
[5] A. Tsoga, A. Gupta, A. Naoumidis, D. Skarmoutsos, P. Nikolopoulos, Ionics 4 (1998) 234.
[6] G.A. Tompsett, N.M. Sammes, O. Yamamoto, J. Am. Ceram. Soc. 80 (12) (1997) 3182.
[7] A. Martínez-Amesti, A. Larrañaga, L.M. Rodríguez-Martínez, A.T. Aguayo, J.L. Pizarro, M.L. Nó, A. Laresgoiti, M.I. Arriortua, J. Power Sources 185 (2008) 401.
[8] S. Simner, M. Anderson, J. Bonnett, J. Stevenson, Solid State Ionics 175 (2004) 79.
[9] K. Yang, J.-H. Shen, K.-Y. Yang, I.-M. Hung, K.-Z. Fung, M.-C. Wang, J. Power Sources 159 (2006) 63.
[10] H.M. Rietveld, J. Appl. Crystallogr. 2 (1969) 65.
[11] J. Rodríguez-Carvajal, Physica B 192 (1993) 55.
[12] J. Rodríguez-Carvajal, Fullprof, Rietveld Pattern Matching Analysis of Powder Patterns, 1994.
[13] Gooden, McCarthy, Penn State University, University Park, PA, USA, ICDD Grant-in-Aid, 1971.
[14] X.-D. Zhou, B. Scarfino, H.U. Anderson, Solid State Ionics 175 (2004) 19.
[15] R.D. Shannon, Acta Crystallogr. A 32 (1976) 751.
[16] W.C. Hagel, J. Am. Ceram. Soc. 48 (1965) 70.
[17] Z. Zhan, T.-L. Wen, H. Tu, Z.-Y. Lu, J. Electrochem. Soc. 148 (5) (2001) A427.